Block Copolymers with Gold Nanoparticles: Correlation between Structural Characteristics and Mechanical Properties

Cesar Mendoza,[†] Torsten Pietsch,[†] Jochen S. Gutmann,[§,||] Dieter Jehnichen,[‡] Nabil Gindy,[†] and Amir Fahmi*,[†]

School of Mechanical, Materials and Manufacturing Engineering. The University of Nottingham, University Park, Nottingham, NG7 2RD, U.K., Institute of Physical Chemistry, University of Mainz, 55099, Mainz, Germany, Max-Planck-Institut für Polymerforschung, Ackermannweg 10, D-55128 Mainz, Germany, and Leibniz-Institut für Polymerforschung Dresden e.V., Hohe Strasse 6, D-01069 Dresden, Germany

Received September 15, 2008; Revised Manuscript Received December 4, 2008

ABSTRACT: We developed a strategy to generate gold nanoparticles within the P4VP domains of a PS-*b*-P4VP diblock copolymer in solid state. An organic−inorganic lamellar structure was obtained through selective incorporation of a gold precursor to the pyridine groups in the P4VP block. Understanding how nanoparticles can affect the linear viscoelastic behavior of a block-copolymer system, could assist in defining a specific processing window for this type of hybrid materials. Herein we compared the rheology of BCPs with and without nanoparticles in order to correlate structure to macroscopic response under mechanical shear. We found that nanoparticles affect significantly the glass transition temperature (T_g) of the P4VP block in which these are sequestered, but also T_{ODT} of the block copolymer system. After reduction and shear alignment, a homogeneous spatial distribution of metallic gold nanoparticles is found within the P4VP phase. These findings are confirmed with scattering methods and transmission electron microscopy measurements. Finally, electric force microscopy scans on the surface of these materials revealed dielectric contrast between the two domains of the hybrid lamellar structure.

1. Introduction

The fabrication of hybrid (organic−inorganic) nanostructured materials is a challenge of both scientific and industrial interest for applications in electronics, photovoltaics, optics and automotive technology.[1] Block copolymers (BCP) are excellent candidates to prepare these hybrid materials due to their characteristic of scalability. Block copolymers provide an organic matrix capable to control shape, dispersion, size distribution, and alignment of nanoparticles selectively incorporated in a specific domain.[2] Organic−inorganic BCPs can be aligned macroscopically using large amplitude oscillating shear (LAOS)[3] as a simple alternative to produce hybrid and highly ordered 3-D patterns.[4]

In the literature, thin film and bulk are the main strategies to prepare nanostructured hybrid materials from block copolymers. Thin film structuring and lithographic techniques usually require multiple-step processes in order to place the inorganic component in a specific spatial array.[5−7] These procedures often take long preparation times and their scalability is relatively limited. On the other hand, few experimental work have addressed the problem of structuring *bulk hybrid block copolymers*, i.e., when the block copolymer microphase separates in the absence of any solvent or substrate interaction and in significantly higher amounts than thin films.

Bulk block copolymer hybrids can be prepared through different strategies: direct polymerization of a monomer-metallic complex,[8] direct assembly of block copolymers with nanoscale metallic species[9] and through chemical coordination with organometallic compounds.[10,11] Pioneer work in this area was developed by the group of Cohen et al,[12] whom introduced for the first time the use of amphiphilic diblock copolymers to synthesize silver nanoparticles *in situ*, building on prior work with water−oil emulsions for synthesis of metallic nanoparticles with controlled sizes.[13] Later on, Möller and coworkers expanded this concept to the PS-*b*-P2VP/$HAuCl_4$ system.[14,15]

The selective incorporation of nanoparticles into BCPs poses numerous complications in order to control the resulting nanostructure. In the context of an *in situ* approach, nanoparticles have relatively wide size distributions, as the reduction of the inorganic precursor occurs in solution.[16] In other cases further aggregation of the nanoparticles occurs in the course of the reduction process taking place in solution.[17] Thus, the resulting morphologies often result irregular and limited to few lamellar periods. Kramer and coworkers developed a strategy that allows both to control the particle size and positioning, through synthesis and stabilization of gold nanoparticles with a PS corona.[18] Once stabilized, the nanoparticles are mixed in solution with a PS-*b*-P4VP, where the PS corona is surrounded by the PS block. The process is followed by solvent evaporation to obtain a new microphase separated hybrid diblock, with gold nanoparticles incorporated into the PS phase. However, the amount of nanoparticles incorporated is relatively limited and often the nanoparticles are present in the interphase between domains.

When inorganic components are incorporated into block copolymers, new structural characteristics affect dramatically the properties in comparison to the pristine component. These structural characteristics range from particle shape, size, interparticle distances, interactions with the polymer, volume fraction, and surface to volume ratio among others; a particular combination of these characteristics will have specific effects on the physical properties. In a series of theoretical papers, Balazs and coworkers found that nanoparticles are capable to switch BCP morphologies from cylindrical to lamellar structures.[19,20] They predicted dramatic influences on the order−disorder transition temperature (T_{ODT})[21] and, studied the influence of nanoparticles in mechanical properties for different nano-

* To whom correspondence should be addressed. E-mail: amir.fahmi@nottingham.ac.uk.
[†] School of Mechanical, Materials and Manufacturing Engineering. The University of Nottingham.
[‡] Leibniz-Institut für Polymerforschung Dresden e.V.
[§] Institute of Physical Chemistry, University of Mainz.
[||] Max-Planck-Institut für Polymerforschung.

10.1021/ma8020954 CCC: $40.75
Published on Web 01/27/2009

particle characteristics.[22] Little efforts have been done however to correlate experimentally structural characteristics of hybrid materials with their mechanical properties in the linear viscoelastic regime. Few groups have reported effects of inorganic components on T_g[23] and T_{ODT}[24] of hybrid diblock copolymers.

The present work is an experimental approach that studies the rheological behavior of a hybrid organic−inorganic material in the linear viscoelastic regime. By comparing the rheology of neat and hybrid diblock copolymers, significant changes were detected on T_g, T_{ODT} and relaxation regimes of the hybrid material. Gold nanoparticles are generated through an *in situ* reduction process, within the solid P4VP domains of a PS-*b*-P4VP diblock copolymer. With these studies in hand, alignment conditions were selected to induce macroscopic alignment via LAOS. XPS scans and powder diffraction tests provided evidence of these processes along the preparation steps. Finally, TEM imaging revealed strong selectivity and homogeneous spatial distribution of the gold nanoparticles.

2. Experimental Part

Materials. A block copolymer of polystyrene-*b*-poly-4-vinylpyridine (PS-*b*-P4VP) from Polymer Source Inc. was used as received. The number average molecular weights are 92 700 g/mol for the PS block and 32 700 g/mol for the P4VP block (polydispersity index 1.13). The corresponding volume fraction for the P4VP block $f_{P4VP} = 0.25$, predicted as hexagonally packed cylinder morphology according to theoretical phase diagrams. The glass transition temperatures for the PS block (111.5 °C) and the P4VP block (188.5 °C) were determined by dynamic mechanical thermal analysis (DMTA). The gold precursor used was chloroauric acid (gold (III) chloride hydrate purum ~50% as Au), purchased from Fluka and used as received. The metal precursor is incorporated in three different ratios with respect to the number of pyridine groups (P4VP:$HAuCl_4$ ratio) in the block copolymer system: 1:1 (PS-*b*-(P4VP/$HAuCl_4$)$_{1.0}$), 4:3 (PS-*b*-(P4VP/$HAuCl_4$)$_{0.75}$), and 2:1 ratio (PS-*b*-(P4VP/$HAuCl_4$)$_{0.50}$). Separate solutions of polymer and precursor were prepared in THF under stirring at 40 °C. Solutions are mixed and stirring continues up to 24 h to ensure effective coordination of the precursor to the 4VP groups. THF is left to evaporate at room temperature under continuous airflow in a fumehood.

Tablet Pressing. After solvent evaporation a dry powder is recovered. For each tablet, 40 mg of powder are pressed between PTFE disks, to form a cylindrical tablet of approximately 0.78 mm thickness and 7.9 mm diameter. The material is heated to 180 °C, with a temperature ramp of 35 °C/min, and compacted at a pressure of 69 kPa for 2 h.

Rheology and Orientation Process. For each test, a tablet of the material is loaded in a parallel plate geometry (8 mm diameter) of an Ares Rheometer (Rheometric Scientific) equipped with a 2KFRTN1 transducer. Rheology characterization is performed under linear viscoelastic regime and conditions of temperature, strain and frequency are selected from the characterization process to run LAOS. In this arrangement, a sinusoidal strain is applied in the form of oscillations with a strain amplitude (γ_0 and frequency ω at a specific temperature T. The test conditions for isochronal experiments are: strain amplitude 0.5%, frequency of 1 Hz and heating rate of 0.5 K/min. For each neat and hybrid materials, rheology characterization is performed before application of LAOS. After analysis of the characterization rheograms, a fresh tablet (non-exposed to LAOS) is loaded in the Rheometer for the shear-alignment experiment. Alignment conditions for the experiment of LAOS are: strain amplitude of 30%, shear frequency 1Hz and temperature of 170 °C. FT-rheology measurements were performed during shearing by means of an external acquisition system based on the specification proposed by Wilhelm et al.[25] Among other applications, this new technique allows to monitor the macroscopic behavior of the material during LAOS, quantifying the degree of non-linear response.[26,27] The response signal of the material during shearing is Fourier transformed so that an intensity spectrum with different harmonic components is obtained. From the intensities ratio of the third harmonic with respect to the fundamental frequency (I_3/I_1) it is possible to monitor the degree of non-linear behavior as a function of time, providing with a mechanical fingerprint for the shear alignment kinetics.

X-ray Photoelectron Spectroscopy. Samples were analyzed using the Kratos AXIS ULTRA with a mono-chromated Al Kα X-ray source (1486.6 eV) operated at 15 mA emission current and 10 kV anode potential. The take off angle for the photoelectron analyzer was 90 deg. The scan area is approximately 300 × 700 μm^2.

Atomic and Electric Force Microscopy. From the ultra microtomed samples, the remaining surface in bulk from the cutting process is scanned in a Dimension IV Nanoscope manufactured by Veeco, under tapping mode, using a silicon cantilever with a resonance frequency of 315 kHz. In electric force microscopy mode, the cantilever is raised 20 nm above the surface of the material. A voltage of 10 V DC is then applied between the silicon substrate and the cantilever. Subsequently a typical scan is run at 0.3 Hz with a resolution of 512 × 512 pixels.

Transmission Electron Microscopy. The samples are previously embedded in epoxy resin. After curing, the samples are microtomed using an Ultramicrotome Leica EM UC6, equipped with a cryo-chamber EMFC6. Diamond knifes for cryo-temperatures (Diatome) were used for both the trimming (model DCTB) and cutting process (model Cryo 45°). The samples were trimmed and cut at −40 °C. From the ultra-microtoming process, 70 nm thick slices are obtained and placed over carbon coated copper grids (400 mesh Cu, from Agar). TEM is performed using a Tecnai T12 Biotwin microscope (FEI Company-UK Ltd.) with electron beam energy of 100 keV.

SAXS *ex Situ*. After the orientation process the sample is quenched to room temperature, complete tablets are extracted from the parallel plates, and exposed to small angle X-ray scattering. An X-ray source (With a three-pinhole collimator to generate a beam with a diameter of 0.1 mm) Rigaku MicroMax 007 with a wavelength of 1.54 Å (Cu Kα) is used. Scattering patterns are recorded in a 2-dimensional area detector (Bruker Highstar) with a sample-to-detector distance of 178 cm. The sample is mounted on a custom-designed translation stage, and alignment of the sample to the X-ray beam is performed by adjusting a laser marker to the desired region of the bulk sample. The small angle diffraction patterns reported were conducted from radial direction, in a small cube of the material taken between 3 and 4 mm from the center of the disk.

3. Results and Discussion

Block-Copolymer/Nanoparticle Systems. Volume Fractions and Gold Precursor. Gold nanoparticles can be generated within the P4VP domains of a PS-*b*-P4VP diblock copolymer by an *in situ* reduction in the solid state. To achieve *in situ* reduction, the gold precursor is coordinated in solution to the pyridine groups ensuring its selective location within the P4VP block. Once the gold precursor is coordinated to each pyridine unit, the PS-*b*-P4VP/$HAuCl_4$ can self-assemble into regularly spaced domains (spheres, cylinders or lamellae). As the gold precursor is now confined to the P4VP block, an *in situ* thermal reduction process generates metallic gold nanoparticles, where the P4VP domain acts as a nanoreactor.

Figure 1 depicts the process of incorporating gold nanoparticles (process A) and its subsequent macroscopic alignment (process B). In process A, a stoichiometric amount of the gold precursor is mixed in solution with a block copolymer of initial volume fraction $f_{P4VP} = 0.25$, corresponding to cylindrical morphology when it is microphase separated. Each pyridine group is protonated with hydrogen from the gold precursor. Following this process, the counter ions of the auric acid coordinate to the 4VP group leading to a hybrid PS-*b*-(P4VP)($HAuCl_4$)$_{1.0}$ (Figure 1 - Step II). The modified P4VP($HAuCl_4$)$_{1.0}$ block can be described in terms of its new volume fraction $f_{P4VP/HAuCl_4}$.

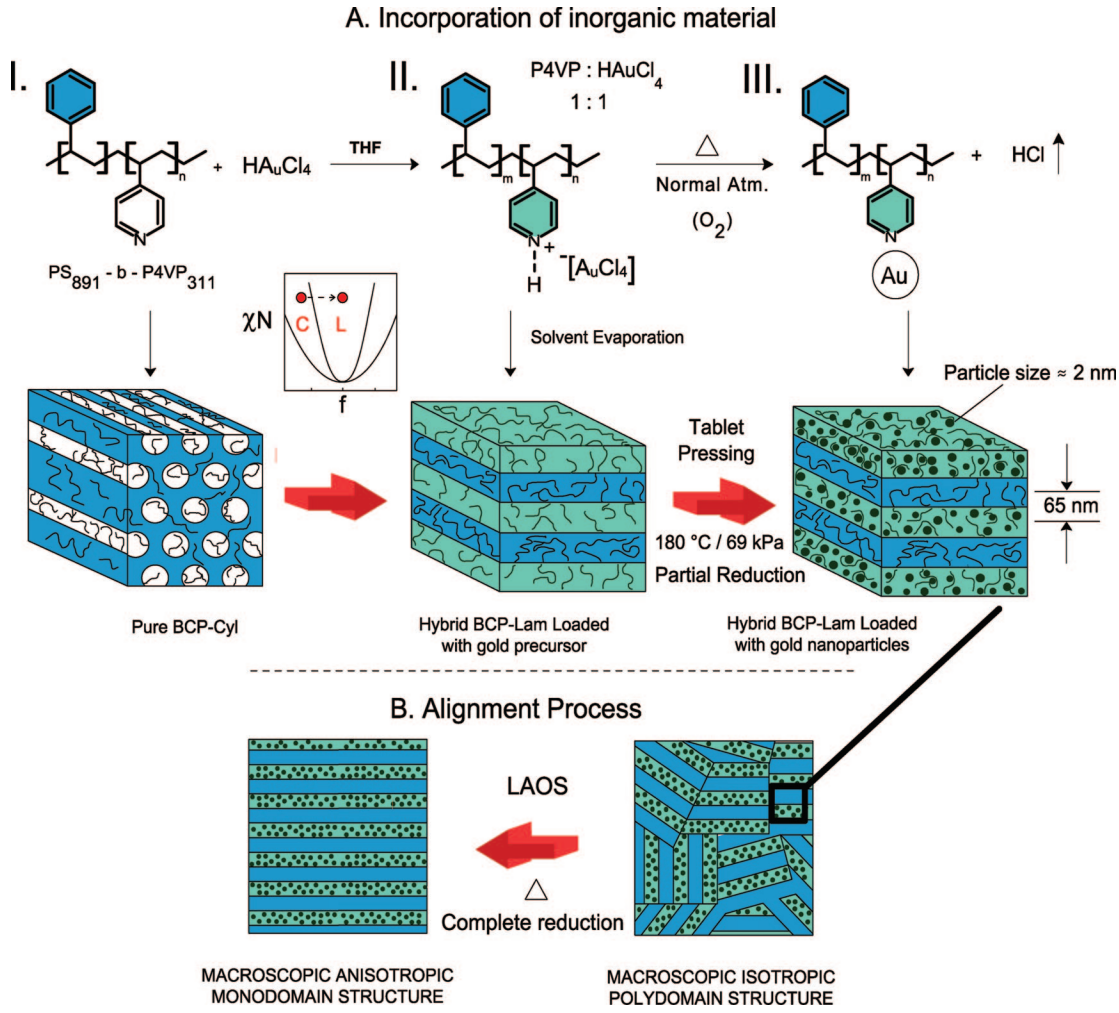

Figure 1. A. Incorporation of inorganic nanoparticles *in situ*. I. The block-copolymer is mixed in solution with tetrachloroauric acid to form PS-*b*-(P4VP/$HAuCl_4$)$_{1.0}$. II. Pyridine groups are protonated and the gold chloride anion coordinates to the positively charged pyridine. The P4VP block is loaded stoichiometrically with gold precursor, which shifts the morphology from cylindrical to lamellar structure. III. After partial reduction process (during tablet pressing), elementary gold atoms aggregate to form metallic nanoparticles. B. The material is sheared under LAOS to macroscopically align the nanostructure. The reduction process continues due to presence of heat, during the alignment process.

During evaporation of THF, the hybrid material microphase separates into a lamellar morphology, as represented in Figure 1, step II. At this point, the lamellar morphology of the bulk material has already been defined by both the interaction parameter $\chi_{PS\text{-}P4VP/HAuCl_4}$ and the new volume fraction $f_{P4VP/HAuCl_4}$. In consequence, the original cylindrical morphology of the neat diblock copolymer has been transferred to lamellar morphology. The self-assembly process is mediated by both the repulsive interaction of PS−P4VP/$HAuCl_4$ contacts during solvent evaporation and the change in volume fraction from the coordination of the gold precursor to the P4VP backbone (Figure 1). Heating the bulk material reduces the gold precursor into elementary atoms of gold that aggregate *in situ*, to form metallic nanoparticles of approximately 2 nm sequestered within the P4VP domains. Therefore, it is virtually impossible to measure the interaction parameter between PS and P4VP/$HAuCl_4$, since varying temperature reduces the gold precursor.

A hybrid block copolymer is obtained (Figure 1, step III), loaded with gold nanoparticles selectively placed in the pyridine block. As there is a limited number of gold atoms with which an individual chain can contribute, in principle, the particles are screened by polymer segments that prevent further particle growth. Finally, the hybrid material is sheared under LAOS (process B, Figure 1) in order to induce macroscopic alignment of the lamellar structure of the hybrid block copolymer.

The reduction process was monitored with a combination of XPS and X-ray powder diffraction measurements. XPS was used to investigate the chemical state of the gold precursor at each step of the preparation process: solvent evaporation, tablet pressing, and mechanical shear. In addition, the presence of crystalline gold is detected from the typical reflections of scattering planes of metallic gold using XRD (see Supporting Information, Figure A). Figure 2a presents XPS high resolution scans in the region corresponding to the binding energies of gold compounds. The scan reveals characteristic emissions corresponding to photoelectrons 4f from the gold compound. For the solvent evaporated sample (i), the spectra can be split into four components: two peaks (at binding energies of 89.3 and 85.6 eV) corresponding to Au^{3+}, and two peaks (86.7 and 82.9 eV) corresponding to Au^0 with relative atomic concentrations of 60.5% and 39.5% respectively. Conversely after the tablet pressing process (ii), an inversion is observed in the concentration of each chemical state, where the remaining Au^{3+} represents 41.4% and the metallic gold Au^0 58.6% of groups. In agreement with previous reports on reduction of gold precursor,[28] this observation demonstrates that the reduction process starts partially during the tablet pressing process. Further heat exposure (during LAOS experiments) produces total conversion to metallic gold, as the spectra in Figure 2b reveals emission components mainly from the Au^0-$4f_{7/2}$ doublet. Finally,

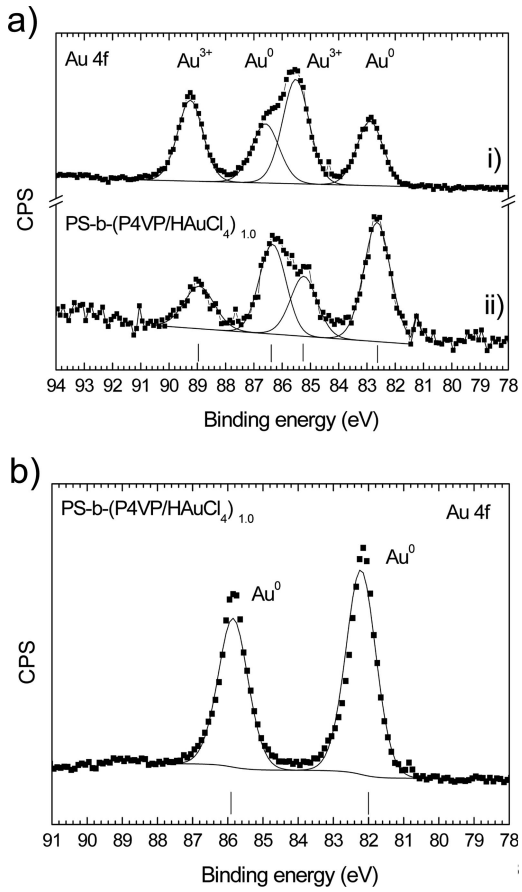

Figure 2. XPS HRES spectra monitoring the *in situ* reduction process: a) Scan on the surface of the hybrid material form PS-*b*-(P4VP/$HAuCl_4$)$_{1.0}$ after evaporation of THF (curve i) and tablet pressing (curve ii). On the solvent evaporated sample, Au^{3+} peaks at binding energies 89.3 and 85.6 eV dominate the relative concentrations compared to the Au^0 peaks. After tablet pressing an inversion in the relative areas under the peaks indicates partial reduction of the Au^{3+}. (b) After application of LAOS, only Au^0 peaks corresponding to binding energies of 85.6 eV (Au-4$f_{5/2}$) and 82.3 (Au-4$f_{7/2}$) are detected.

Figure 3 presents a HRTEM micrograph of the material where characteristic fringes demonstrate the presence of the crystalline gold within the P4VP domain.

Even though it is certain that P4VP domains sequester metallic gold nanoparticles, side products of the reduction process are released from the material.

$$\mathrm{Py{-}H^+ + [AuCl_4]^- \xrightarrow{O_2,\,\Delta} Au^0 + Cl_2(g) + 2HCl(g)}$$

Along the investigated samples and TEM micrographs, we did not find any bubbles or cavities indicating presence of gaseous compounds in the material. Thermogravimetric Analysis (TGA) experiments demonstrate that most of the side products from the reduction process are released from the material (see Supporting Information, Figure B). Thus, traces detected with XPS do not exceed 0.5% in weight of the material.

TEM micrographs of the hybrid system are presented in parts a and b of Figure 4. The structure obtained has unprecedented contrast and consistent regularity in the lamellar spacings of both blocks. The electronic contrast of the metallic gold nanoparticles allows their distinction from the PS-rich regions, without the use of staining agents. From a series of TEM micrographs, the morphology obtained showed highly regular periodicity (lamellar structure) and homogeneous distribution of nanoparticles along the P4VP block. Differences in lamellar

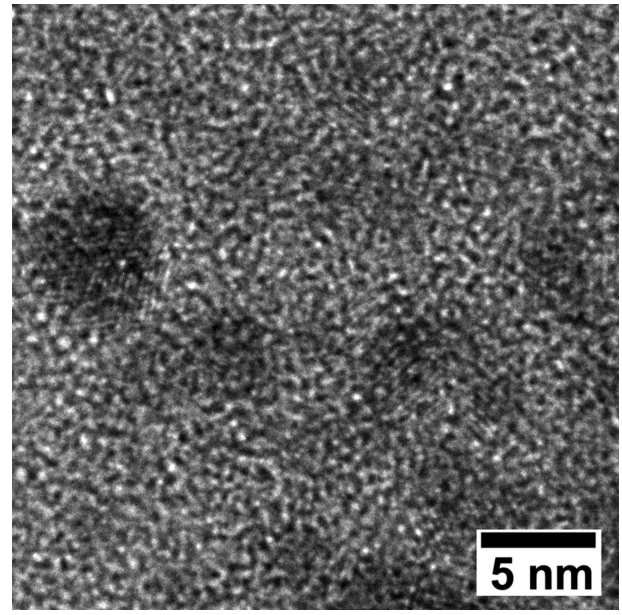

Figure 3. HRES−TEM micrograph of a microtomed section of the hybrid material PS-*b*-(P4VP/$HAuCl_4$)$_{1.0}$. Fringes characteristic of a crystalline structure demonstrate the presence of gold nanoparticles in the hybrid material after thermal reduction.

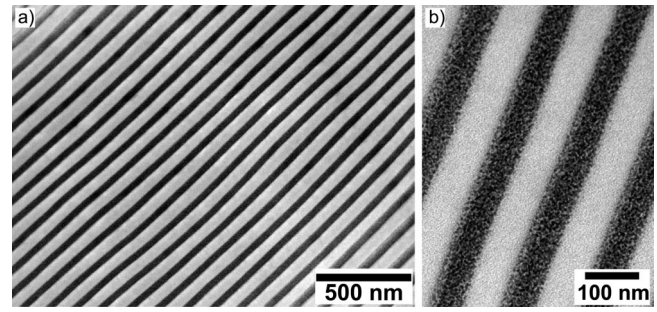

Figure 4. Transmission electron micrograph of non-stained microtomed sections of the hybrid material PS-*b*-(P4VP/$HAuCl_4$)$_{1.0}$ after the orientation process. (a) The clear contrast of the phases confirms the strong selectivity on the incorporation of the metallic precursor. In addition, a highly ordered lamellar structure is presented in an area of approximately 2 μm^2. (b) The zoomed area emphasizes the selective confinement of the metallic nanoparticles and their homogeneous distribution within the P4VP phase.

periods were found for different batches of the material, but these did not exceed ~10% in all cases.

The use of reduction agents in solution (such as $NaBH_4$) does not lead to such self-assembled morphology after solvent evaporation process. Two experiments corroborate this statement. In the first experiment, the hybrid PS-*b*-(P4VP/$HAuCl_4$)$_{1.0}$ is prepared in solution with THF, whereas in the second experiment, the hybrid is prepared in solution with toluene. Addition of sodium borohydride to both solutions reduces the gold precursor to metallic gold. Since THF is a common solvent for both P4VP/$HAuCl_4$ and PS blocks, the chains are relatively extended in solution. For this reason, gold nanoparticles can aggregate into big clusters during the reduction process. In contrast, toluene is a selective solvent for the PS block. Thus, the polar P4VP block contracts to minimize contacts with toluene, leading to a micellar solution. Upon addition of $NaBH_4$, the micelle core (P4VP) protects the generation of small nanoparticles, surrounded by a PS corona. (Previously demonstrated by Moller, Spatz. Et al[14,15] in thin films) (see Supporting Information, Figures D and E). These findings confirm that during solvent evaporation, the BCP self-assemble into mi-

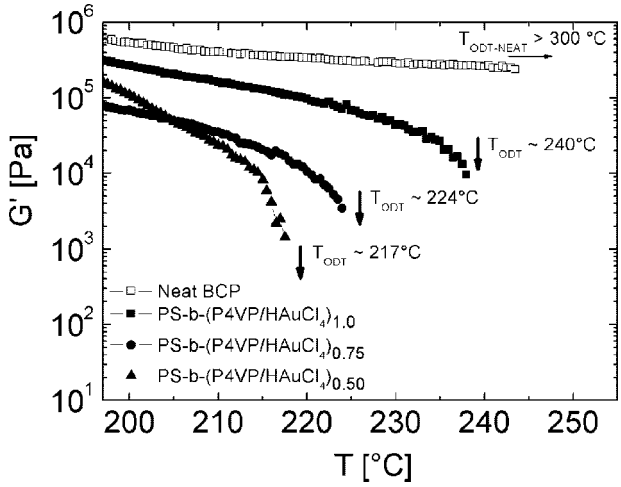

Figure 5. Temperature dependence of the elastic modulus G' at < = 1 Hz for both hybrid and neat materials. The order−disorder transition temperature for each material is indicated: (□) neat PS-*b*-P4VP, T_{ODT} not detected; (■) hybrid PS-*b*-(P4VP)(HAuCl$_4$)$_{1.0}$, T_{ODT} = 240 °C; (●) hybrid PS-*b*-(P4VP)(HAuCl$_4$)$_{0.75}$, T_{ODT} = 224 °C; (▲) PS-*b*-(P4VP)-(HAuCl$_4$)$_{0.5}$, T_{ODT} = 224 °C.

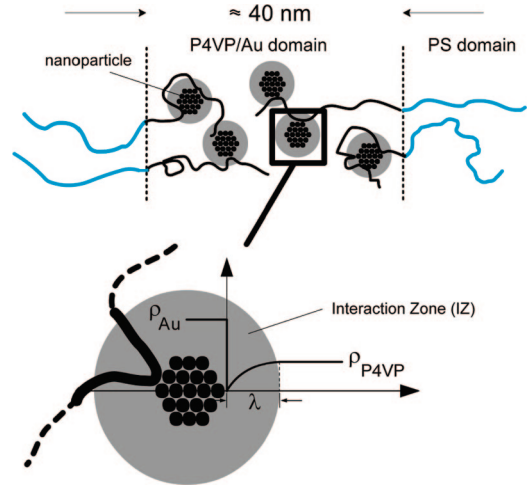

Figure 6. Schematics of the interaction zone (IZ) within the P4VP block. The IZ is represented by the shaded circular area surrounding the nanoparticles. The zoomed area, represents the polymer density-profile around the nanoparticles.

crophase separated morphologies only if the gold precursor remains coordinated in the P4VP blocks. Such self-assembly phenomenon is not present when reduction agents are used.

From particle analysis of Figure 4b (see Supporting Information, Figure C), the average particle radius (R_P) is around 0.9 nm. On the other hand, the end-to-end (R_0) distance is 5 nm for the polymer chain. Thus, the ratio $R_P/R_0 = 0.2$ corresponds to approximately to the case for small particle size, according to Balazs' model.[20] For a volume fraction of nanoparticle content $\phi_P = 15\%$, theoretical calculations predict an edge assembled morphology, across the block containing the nanoparticles. For the hybrid system that concerns this report, the volume fraction of gold content (ϕ_{Au}) corresponds to a 2.6%, (assuming 100% conversion of the gold precursor). This low nanoparticle content explains the relatively homogeneous distribution of nanoparticles along the P4VP lamellae, as inferred from the theoretical prediction from Balazs. In addition, particle growth is confined to the P4VP domains, so that nanoparticle segregation is already high along the P4VP block. With the present method the nanoparticle content is limited to the number of precursor molecules coordinated to functional groups (4VP) within the P4VP block.

Linear Viscoelasticity of Hybrid and Neat Block Copolymers Compared. *Nanoparticle Effect on the Order−Disorder Transition Temperature.* The order−disorder transition temperature (T_{ODT}) is evaluated for both pure and hybrid block-copolymer systems. For the sake of comparison, two additional hybrid systems are presented for this analysis: one with 75% of P4VP groups coordinated with gold precursor (PS-*b*-(P4VP)(HAuCl$_4$)$_{0.75}$) and a second one with 50% (PS-*b*-(P4VP)(HAuCl$_4$)$_{0.50}$). Conditions for the isochronal experiment are as follows: frequency 1 Hz, temperature range from 200 to 250 °C, and strain amplitude 0.5% (linear regime) (Figure 5). In the course of the experiment, the neat material preserves its viscoelastic character as T_{ODT} is not detected within the temperature range tested; the experiment was stopped at 245 °C to avoid oxidative effects on the neat polymer material. This behavior is expected considering a recent report from Zha[29] and coworkers, where T_{ODT} for PS-*b*-P4VP systems is estimated theoretically around 900−1000 °C. Conversely, the hybrid PS-*b*-(P4VP)(HAuCl$_4$)$_{1.0}$ starts purely viscous flow around 240 °C, to the point that it flows out of the parallel plates. A steep decrease in G' is a typical indication of an order−disorder transition, as it has been reported in extensive diblock copolymer systems.[30] The systems PS-*b*-(P4VP)(HAuCl$_4$)$_{0.75}$ and PS-*b*-(P4VP)(HAuCl$_4$)$_{0.50}$ also exhibit consistent shifts in T_{ODT}, identified with abrupt drops of G' at 224 °C and 217 °C respectively.

Chervanyov and Balazs explained theoretically the reasons for T_{ODT} shift by defining a depletion layer surrounding the nanoparticles.[21] The depletion layer possess the following characteristics: (i) The density of repeating units is zero at the nanoparticle's surface and, in consequence, there is a reduction of contacts among repeating units near the surface. Due to chain connectivity, the change in density profiles is a smooth function within the depletion layer, until it reaches the density of bulk domains (P4VP domains in the present case, Figure 6). (ii) Density fluctuations cause a non-uniform distribution of repeating units inside the depletion layer, thus ρ_{P4VP} is reduced. (iii) At smaller nanoparticle size, there is a higher surface to volume ratio, implying a larger number of density fluctuations in the bulk domains. Chervanyov and Balazs predict the highest shift on T_{ODT} at small volume fractions of nanoparticle content (5%) and small particle size. This reasoning suggests that the structural characteristics of the present system must be comparable to the mentioned model in order to induce the observed T_{ODT} shift. Mainly due to the presence of small nanoparticles (1.6 nm) in a relatively small volume fraction ($\phi_{Au} = 2.6\%$).

From a practical perspective, the results are in agreement to the work of Wiesner and coworkers, where a shift of 23 °C in T_{ODT} is reported for PS-*b*-PI systems with rodlike clay nanoparticles.[24] As an underlying implication, hybrid materials could be processed at lower temperatures than neat diblock copolymer systems and, depending on the molecular weight, without compromising chain degradation.

Nanoparticle Effect on the Glass Transition Temperature. Now we compare the flow of both the hybrid and neat block copolymer systems, keeping constant molecular weight. Figure 7 presents isochronal measurements of the elastic modulus (G') and loss tangent ($\tan\delta = G''/G'$) versus temperature. Similarly to the previous effect, T_g of P4VP block ($T_{g\text{-}P4VP}$) decreased from 188.5 °C to 164.0 °C respectively. Not only on the P4VP block but also on the PS block the glass transition ($T_{g\text{-}PS}$) shifts from 111.5 °C for the neat material to 104.5 °C for the hybrid. Shortly after $T_{g\text{-}PS}$, the hybrid material exhibits a rubbery plateau where values of G' for the hybrid BCP are higher compared to G' of the neat BCP. This behavior occurs in a temperature window from 100 until 180 °C after

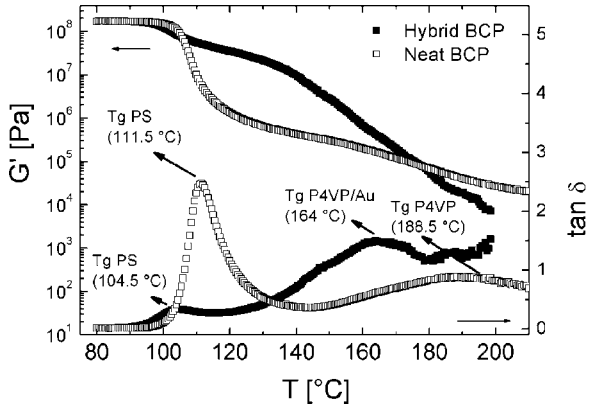

Figure 7. Isochronal temperature ramp in the linear viscoelastic regime. The elastic modulus (G') and the loss tangent (tan δ) are shown for the hybrid PS-*b*-(P4VP/$HAuCl_4$)$_{1.0}$ and neat block copolymers. Test conditions are as follows: strain amplitude of 0.5%, frequency of 1 Hz, and heating rate of 0.5 K/min. Note the shift in T_g for the hybrid system.

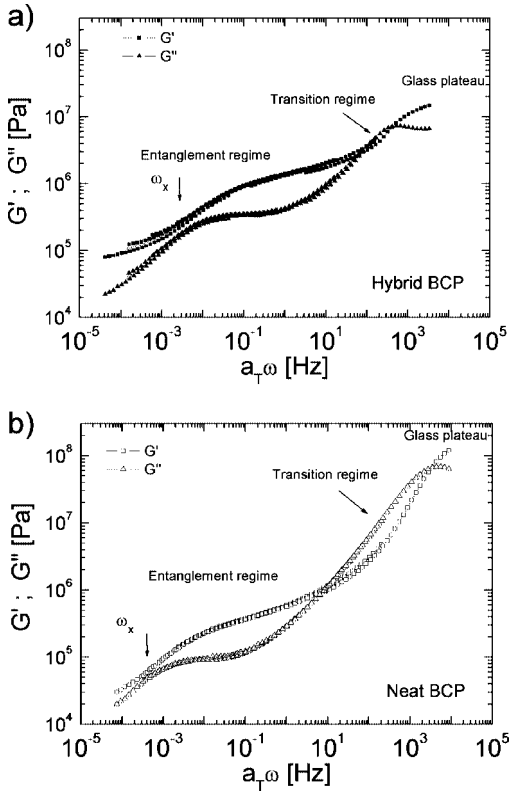

Figure 8. Master curves for storage (G') and viscous moduli (G'') for (a) hybrid BCP PS-*b*-(P4VP/$HAuCl_4$)$_{1.0}$ (filled symbols) and (b) neat material PS-*b*-P4VP (open symbols). Data were built using time−temperature superposition from frequency sweep tests at temperatures from 110 °C to 170 °C, with intervals of 10 °C each test. Reference temperature T_0 = 130 °C.

which G' for the hybrid material starts to drop below the neat BCP.

The observed T_g shift is consistent with observations from Ash and coworkers for PMMA/alumina nanoparticle systems.[31] In that report T_g drops 25 °C for low particle weight fractions and with particle size from 10 to 38 nm. Ash and coworkers suggests the existence of an IZ, within the polymer chains and the nanoparticles. This zone would be responsible for enhancing (or hindering) the mobility (in terms of conformational changes) of the polymer matrix with respect to the nanoparticles. Following the ideas of Chervanyov and Balazs on the theoretical

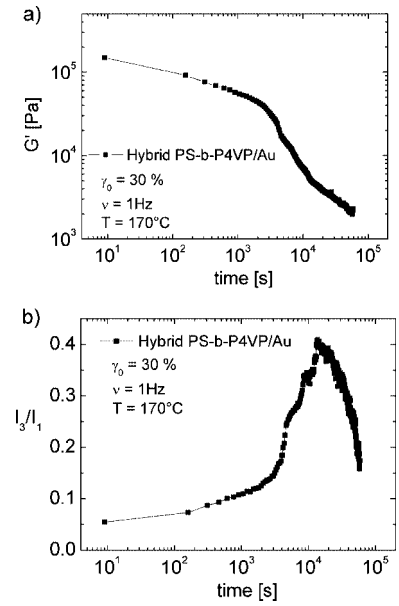

Figure 9. (a) Time dependence of the elastic modulus for the hybrid BCP PS-*b*-(P4VP/$HAuCl_4$)$_{1.0}$ during application of LAOS. Strain amplitude was 30%, at a temperature of 170 °C and frequency of 1Hz. (b) Corresponding non-linear monitoring of the third harmonic from FT-Rheology spectra.

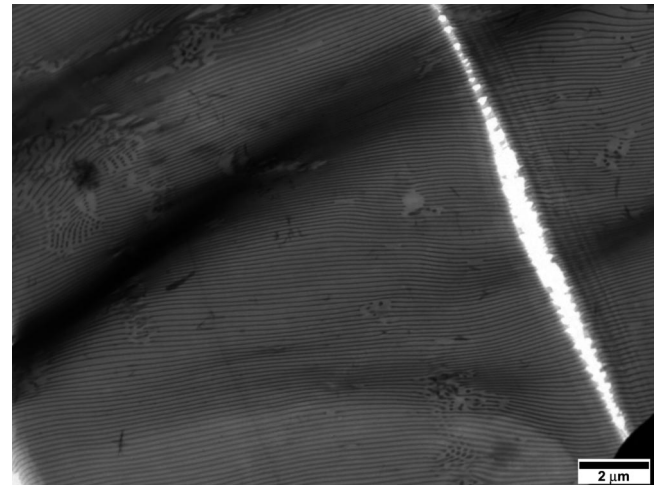

Figure 10. Transmission electron micrograph of the hybrid material PS-*b*-(P4VP/$HAuCl_4$)$_{1.0}$ after shearing. Notice the highly aligned structure along 20 μm, evidence of the possibility to induce macroscopic alignment of the hybrid material.

depletion layer (equivalent to the IZ), we can picture this layer as a spherical shell of thickness λ. (represented as a shaded circle around the nanoparticles, Figure 6). Where λ is proportional to the Kuhn's length segment of the P4VP chain (b = 0.68 nm).[32]

We suggest two main contributions to the generation of free volume: the first is due to generation of the densely packed crystalline structure of the metallic nanoparticles, and if the argument of Chervanyov and Balazs holds, the second contribution comes from a volume of reduced density of P4VP near the nanoparticles' surface (Figure 6). This reduced density explains the existence of additional free volume surrounding the nanoparticles. The effect of additional free volume on chain mobility has been reported for many other contributions such as presence of plasticizer, chain ends from low molecular weight chains among other effects.[33] For these reasons as the temperature is increased, the available free volume promotes conformational changes in the polymer backbone, resulting in an overall lower glass transition within the P4VP block. This effect continues

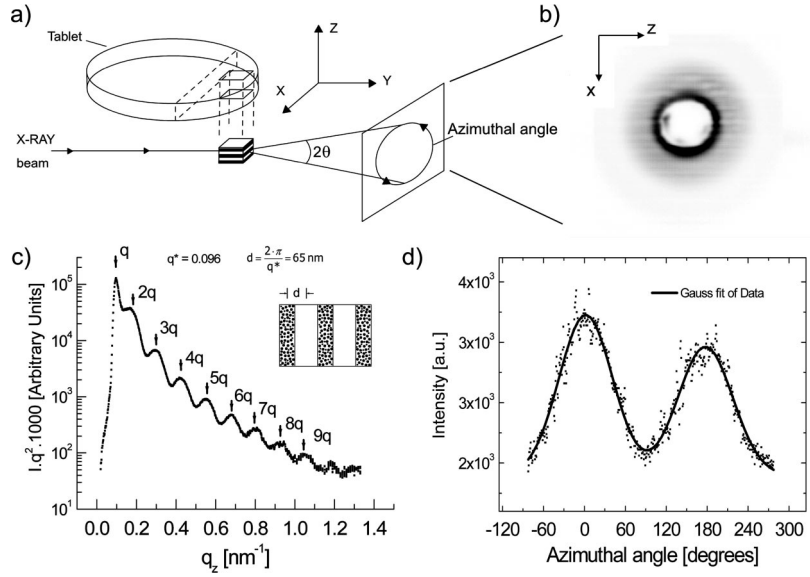

Figure 11. (a) Schematics of a tablet of the material and the positioning for SAXS characterization. X: shear direction, Y: X-ray beam. A cube from the tablet was cut and exposed to the X-ray beam in radial direction with respect to the center of the tablet. (b) 2D scattering map of a hybrid PS-*b*-(P4VP/$HAuCl_4$)$_{1.0}$ di-block-copolymer system sheared with large amplitude oscillating shear. (c) Small angle diffraction pattern confirms the lamellar morphology of the hybrid material. Up to nine equally spaced intensity maxima are identified by the ratios $1q$:$2q$:$3q$..., where q_z (scattering vector) is given by $q_z = (4\pi/\lambda)\sin\theta$, 2θ being the scattering angle and $\lambda_{CuK\alpha} \approx 1.54$ Å. (d) Azimuthal intensity distribution of the 2D pattern (q-range: integrated over the 5th layer reflection).

after 170 °C, when G' values for the hybrid material start to drop with respect to G' of the neat BCP (Figure 7).

Nanoparticle Effect on the Linear Viscoelastic Behavior. Figure 8 presents master curves of the elastic and loss modulus versus frequency. The data is fitted to the Williams−Landel−Ferry model at a reference temperature of 413 K. Differences in the mechanical response are analyzed only from the presence of the nanoparticles at constant molecular weight of the BCP, even though both neat and hybrid materials possess different nanostructures (Figure 1).

At high frequencies, there is a glass plateau regime for both hybrid (Figure 8a) and neat materials (Figure 8b), mainly attributed to the relaxation of the PS block. However, the hybrid diblock exhibits lower moduli when compared to the neat system. The transition regime is considerably shorter in the case of the hybrid diblock. Whereas the neat system can relax in the transition regime owing to the rubbery PS block, the hybrid system undergoes a shorter relaxation to exhibit again elastic-dominant behavior along the entanglement regime. The entanglement regime starts at frequencies one decade higher for the hybrid system in comparison with the neat material. At frequencies around 10^{-3} Hz G' and G'' approximate to each other but no crossover frequency (ω_x) is observed in both cases. However, in the case of the hybrid BCP the separation is more obvious, where both G' and G'' exhibit higher values in comparison to the neat material.

Values of G' for the hybrid BCP are higher than those of the neat BCP, which means a stiffer BCP. This observation agrees with the higher G' found in the temperature test in Figure 7. This evidence suggests that at low frequencies (temperatures around $T_{g\text{-P4VP}}$) the nanoparticles act as anchoring points, by hindering the disentanglement/reptation of chains. The anchoring effect could arise from 4VP segments in contact with the surface of the gold nanoparticles, within the interaction zone, as it has been demonstrated that there is a favorable interaction between 4VP groups and gold surfaces.[18,34] We suggest that this affinity hinders mobility of the bulk P4VP block, thus, increasing G'.

Alignment of Block Copolymer/Nanoparticles Systems in the Non-Linear Regime. Even in the non-linear region, the dynamics of block copolymers under shear are related to the frequency dependence in the linear viscoelastic regime.[35] A delicate interplay of frequency, temperature and strain defines both the quality of orientation and the type of alignment. In addition, the presence of the nanoparticles adds an even more complex dynamics governing domain alignment and defect migration, as shown in the previous paragraphs.

Two key parameters to take into account when deciding a set of alignment conditions are: the glass transition temperatures of both blocks and the order−disorder transition of the hybrid system. We restricted the shearing temperature below the order−disorder transition of the hybrid diblock copolymer presented in Figure 5 ($T_{ODT} \sim 240$ °C). Shearing at temperatures close to T_{ODT} could perturb the selective location of the metallic nanoparticles. Large amplitude oscillating shear was applied at 170 °C and deformation amplitude $\gamma_0 = 30\%$, in order to ensure non linear behavior during the alignment (see Supporting Information, Figure F). Experimentally, a frequency of 1 Hz also proved to be an appropriate frequency to induce alignment in LAOS for alignment of lamellar PS-*b*-P4VP system.[4]

The hybrid system shows a significant decrease of G' of two orders of magnitude (Figure 9a) declining until the end of the experiment (17 h). Regarding the response of the hybrid diblock-copolymer, the degree on non-linearity is measured via monitoring the relative intensity of the third harmonic (I_3/I_1) in the response signal with respect to the fundamental frequency (Figure 9b). Non-linear response starts with values of $I_3/I_1 = 0.05$, building up to 0.4 in the course of 3 hours of shearing. These results are in agreement with previous reports on orientation of diblock copolymer systems coupled with amphiphiles.[36] The strong increase in non-linear character might be attributed to the complexity of the flow, from the intermolecular processes taking place within the IZ in the P4VP block. After 3 hours of shearing, I_3/I_1 reaches values around 0.15 non-linearity, indicating effective grain-alignment as suggested by Wilhelm and coworkers for diblock copolymer systems.[25]

Visual confirmation of the aligned structure is presented in a TEM micrograph on Figure 10. The macroscopic character of

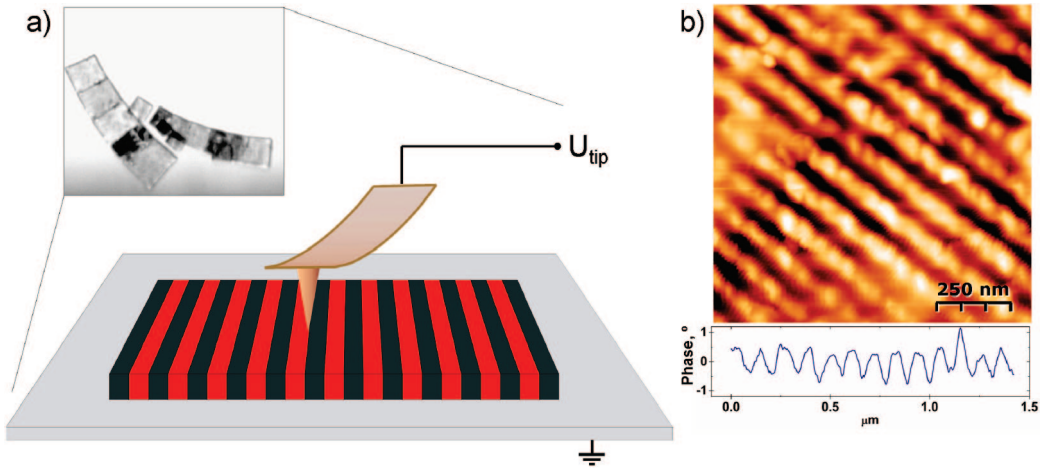

Figure 12. Electric force microscopies scan over the surface of the hybrid BCP PS-*b*-(P4VP/$HAuCl_4$)$_{1.0}$. (a) Optical photograph of microtomed slices of the hybrid material deposited on silicon wafers and schematics of the scanning process. A voltage of 5V-DC is applied between the substrate and the cantilever holder while a silicon tip oscillates at 20 nm height from the surface. (b) Phase image revealing the dielectric contrast between PS (dark areas) and P4VP/Au (bright areas).

the alignment process is evident from nearly a single lamellar domain with continuous alignment along 20 μm in length across the micrograph. After application of LAOS, the material is taken out from the parallel plates for evaluation *ex situ*, of both structure and macroscopic alignment.

Characterization of the Hybrid Material After LAOS. An X-ray beam is directed over a section of the tablet from radial direction, as depicted schematically in Figure 11a. A 2D scattering map for the hybrid material is presented in Figure 11b.

Integrating the scattering map first on the 2θ direction provides one with a typical SAXS profile of block copolymer, as presented in Figure 11c. Lamellar structure is confirmed from the position of Bragg reflections identified in a ratio $1q$:$2q$:$3q$..., with multiplicities up to the 9th order. This result clearly indicates the highly regular lamellar spacing (in terms of the new microphase separation process) of the hybrid material. On the other hand, integrating over the azimuthal angle on the 5th reflexion leads to intensity peaks presented in Figure 11d, which can be used to evaluate the degree of orientation. Two azimuthal peaks at 0° and 180° suggest that there is preferential macroscopic alignment of the domains of the hybrid block copolymer. Further improvement of the alignment can be achieved optimizing the combination of temperature, frequency and strain conditions.

On the structural side, the lamellar period of the hybrid BCP determined from analysis of the SAXS profile was found in good agreement with TEM measurements. Analysis of the first Bragg reflexion of the SAXS profile on Figure 11c provides an average size of the domain period of 65nm. On the other hand, a similar average lamellar period is obtained by taking local measurements on the TEM micrograph in Figure 4b. Considering that SAXS represents an average of the scattering volume in bulk and, provided that the lamellar period matches between both techniques, we can conclude that the particles must reside only in the P4VP phase. Since gold nanoparticles are not compatible with PS,[34] we do not expect (and so far have not observed) any migration of nanoparticles to the PS domains.

In the literature, macroscopic alignment is reported with scattering volumes similar to the one tested in the present investigation. Moreover, in the case of parallel plate geometry, there is a distribution of strains starting from 0% deformation in the center of the geometry ending with the commanded 30% strain in the edge of the plates. Considering that the x-ray beam diameter is of approximately 0.1 mm and sample thickness 0.78 mm, the scattering experiment averages orientations from a volume of 0.02 mm^3. This volume corresponds to the bulk sample at a radial position between 3 and 4 mm from the center of the plates. Comparing the domain sizes (65 nm) and the scale of the probe volume (0.02 mm^3), the results indicate a high degree of alignment in the hybrid material. However, alignment from LAOS provides the proof of concept, as this material can be extruded in fibers resulting in a more uniform alignment across the sample.

Figure 12 presents electric force microscope (EFM) scans on the surface of the bulk material. The optical photograph shows 200 nm thick microtomed slices of the material, deposited on the surface of a silicon wafer (Figure 12a). A DC voltage is applied between the substrate and the cantilever as the cantilever oscillates at 20nm above the surface. This voltage induces local electric fields in the material as the tip scans above the domains. The phase shift between the excitation resonance frequency and the cantilever's response provides a measure of the differences in dielectric properties within each domain.

From the scan in Figure 12b, it is clear that the induced electric field does not fade sharply at the interphase of the lamellae. The phase shift in the dark areas is more homogeneous than the one in the bright areas. We infer that the dark areas which exhibit homogeneous phase shift correspond to the PS domains. In contrast, the brighter areas exhibit non-homogeneous phase shift due to the different dielectric environments present across the P4VP/gold-nanoparticle domains. In addition, topological features from the microtoming process create a non-homogeneous electric field, especially in the interphase between both materials. However, this measurement corroborates the dielectric contrast between both PS and P4VP/Au domains, making the hybrid material a potential candidate for photonic band gap devices.

4. Conclusions

We have demonstrated the *in situ* character of a reduction process to generate gold nanoparticles selectively within a specific block (P4VP) of a diblock copolymer (PS-*b*-P4VP). Subsequently a standard shearing process (LAOS) proved successful to produce macroscopically aligned hybrid block copolymers.

The order−disorder transition temperature is dramatically affected with just 2.6 vol % of nanoparticles. The glass transition temperature of both PS and the P4VP blocks exhibit a shift to lower values with respect to the neat material in agreement with

previous studies. In the linear viscoelastic regime, nanoparticles extend the entanglement region and produce an increase in the elastic modulus with respect to the neat material. With large amplitude deformations, the response of the hybrid material results in a non-linear character possibly attributed to irregularities from the presence of the nanoparticles. These observations suggest that the flow behavior of hybrid systems results from a complex combination of competing effects: firstly the presence of free volume arising from a non-homogenous polymer density profile around the nanoparticles that increase chain mobility. Second, an anchoring effect that partially hinders chain mobility, owed to the known affinity of pyridine segments in contact with the gold surfaces. Further work will follow in order to study these tendencies for different morphologies, particle content, and different inorganic precursors. Potentially, these domains could be used as multicontacting tracks, characteristic to be explored in future work, through local transport measurements.

The simplicity of this concept relies in that no special hardware would be required to fabricate these 3D-ordered organic−inorganic nanostructures. Once the material is obtained with precursor previously coordinated right after polymerization, a standard production process such as extrusion can induce alignment and reduction simultaneously.

Acknowledgment. We acknowledge the financial support of the UK-EPSRC through their Nottingham NIMRC and the 3D-MINTEGRATION Grand Challenge project. We thank Michael Bach (MPIP-Mainz/Germany) for the strong support for SAXS measurements.

Supporting Information Available: Figures showing a WAXS diffraction pattern for the material, a TGA experiment, histogram of particle sizes, TEM pictures, and a plot of dynamic strain tests. This material is available free of charge via the Internet at http://pubs.acs.org.

References and Notes

(1) Balazs, A. C.; Emrick, T.; Russell, T. P. *Science* **2006**, *314*, 1107–1110.
(2) Bockstaller, M. R.; Mickiewicz, R. A.; Thomas, E. L. *Adv. Mater.* **2005**, *17*, 1331–1349.
(3) Keller, A.; Pedemont, E.; Willmout, F. M. *Kolloid Z. Z. Polym.* **1970**, *238*, 385.
(4) Mendoza, C.; Pietsch, T.; Gindy, N.; Fahmi, A. *Adv. Mater.* **2008**, *20*, 1179–1184.
(5) Jeong, S. J.; Xia, G.; Kim, B. H.; Shin, D. O.; Kwon, S. H.; Kang, S. W.; Kim, S. O. *Adv. Mater.* **2008**, *20*, 1898–1904.
(6) Thurn-Albrecht, T.; Schotter, J.; Kastle, G. A.; Emley, N.; Shibauchi, T.; Krusin-Elbaum, L.; Guarini, K.; Black, C. T.; Tuominen, M. T.; Russell, T. P. *Science* **2000**, *290*, 2126–2129.
(7) Fahmi, A. W.; Braun, H. G.; Stamm, M. *Adv. Mater.* **2003**, *15*, 1201–1204.
(8) Massey, J. A.; Winnik, M. A.; Manners, I.; Chan, V. Z. H.; Ostermann, J. M.; Enchelmaier, R.; Spatz, J. P.; Moller, M. *J. Am. Chem. Soc.* **2001**, *123*, 3147–3148.
(9) Lin, Y.; Boker, A.; He, J.; Sill, K.; Xiang, H.; Abetz, C.; Li, X.; Wang, J.; Emrick, T.; Long, S.; Wang, Q.; Balazs, A.; Russell, T. P. *Nature* **2005**, *434*, 55–59.
(10) Thomas, J. R. *J. App. Phys.* **1966**, *37*, 2914.
(11) Grubbs, R. B. *J. Polym. Sci., Part A: Polym. Chem.* **2005**, *43*, 4323–4336.
(12) Cheong Chan, Y. N.; Schrock, R. R.; Cohen, R. E. *J. Am. Chem. Soc.* **1992**, *114*, 7295–7296.
(13) Kurihara, K.; Kizling, J.; Stenius, P.; Fendler, J. *J. Am. Chem. Soc.* **1983**, *105*, 2574–2579.
(14) Spatz, J. P.; Mossmer, S.; Moller, M. *Chem. Eur. J.* **1996**, *2*, 1552–1555.
(15) Mossmer, S.; Spatz, J. P.; Moller, M.; Aberle, T.; Schmidt, J.; Burchard, W. *Macromolecules* **2000**, *33*, 4791–4798.
(16) Hashimoto, T.; Harada, M.; Sakamoto, N. **1999**, *32*, 6867−6870.
(17) Sohn, B. H.; Seo, B. H. *Chem. Mater.* **2001**, *13*, 1752–1757.
(18) Kim, B. J.; Bang, J.; Hawker, C. J.; Kramer, E. J. *Macromolecules* **2006**, *39*, 4108–4114.
(19) Lee, J. Y.; Shou, Z. Y.; Balazs, A. C. *Macromolecules* **2003**, *36*, 7730–7739.
(20) Thompson, R. B.; Ginzburg, V. V.; Matsen, M. W.; Balazs, A. C. *Science* **2001**, *292*, 2469–2472.
(21) Chervanyov, A. I.; Balazs, A. C. *J. Chem. Phys.* **2003**, *119*, 3529–3534.
(22) Buxton, G. A.; Balazs, A. C. *Phys. Rev. E* **2003**, *67*, 031802.
(23) García, I.; Tercjak, A.; Zafeiropoulos, N. E.; Stamm, M.; Mondragon, I. *Macromol. Rapid Commun.* **2007**, *28*, 2361–2365.
(24) Jain, A.; Gutmann, J. S.; Garcia, C. B. W.; Zhang, Y. M.; Tate, M. W.; Gruner, S. M.; Wiesner, U. *Macromolecules* **2002**, *35*, 4862–4865.
(25) Wilhelm, M. *Macromol. Mater. Eng.* **2002**, *287*, 83–105.
(26) Wilhelm, M.; Reinheimer, P.; Ortseifer, M. *Rheol. Acta* **1999**, *38*, 349–356.
(27) Wilhelm, M.; Reinheimer, P.; Ortseifer, M.; Neidhofer, T.; Spiess, H. W. *Rheol. Acta* **2000**, *39*, 241–246.
(28) Jaramillo, T. F.; Baeck, S. H.; Cuenya, B. R.; McFarland, E. W. *J. Am. Chem. Soc.* **2003**, *125*, 7148–7149.
(29) Zha, W.; Han, C. D.; Lee, D. H.; Han, S. H.; Kim, J. K.; Kang, J. H.; Park, C. *Macromolecules* **2007**, *40*, 2109–2119.
(30) Gupta, V. K.; Krishnamoorti, R.; Chen, Z.-R.; Kornfield, J. A.; Smith, S. D.; Satkowski, M. M.; Grothaus, J. T. *Macromolecules* **1996**, *29*, 875–884.
(31) Ash, B. J.; Siegel, R. W.; Schadler, L. S. *J. Polym. Sci., Part B: Polym. Phys.* **2005**, *43*, 114–114.
(32) Clarke, C. J.; Eisenberg, A.; La Scala, J.; Rafailovich, M. H.; Sokolov, J.; Li, Z.; Qu, S.; Nguyen, D.; Schwarz, S. A.; Strzhemechny, Y.; Sauer, B. B. *Macromolecules* **1997**, *30*, 4184–4188.
(33) Sperling, L. H. *Introduction to Physical Polymer Science*, 2nd ed.; Wiley: New York, **1985**.
(34) Kunz, M. S.; Shull, K. R.; Kellock, A. J. *J. Appl. Phys.* **1992**, *72*, 4458–4460.
(35) Zhang, Y.; Wiesner, U. *Macromol. Chem. Phys* **1998**, *199*, 1771–1784.
(36) Fahmi, A. W.; Brunig, H.; Weidisch, R.; Stamm, M. *Macromol. Mater. Eng.* **2005**, *290*, 136–142.

MA8020954